ADVANCED ELECTRONIC MATERIALS Open Access
www.advelectronicmat.de

Study on Growth of Tungsten Bronze Phase from Niobate Perovskite Ceramics in Controlled Atmosphere for Photoferroelectric Applications

Xi Shi, Yang Bai, Christoph Wichmann, Michael Moritz, Michel Kuhfuß, Christian Papp, and Neamul H Khansur**

Recent research has found that by introducing A-site deficiency into Ba/Ni co-doped (K,Na)NbO_3 ABO_3-type perovskite, a beneficial interface for photoferroelectric applications is formed between the perovskite and tungsten bronze (TB) phases. To date, such an interface is formed only spontaneously, and the growth mechanism of the TB phase in the perovskite phase is unclear. This work investigates controlled interface formation using KNBNNO ($K_{0.50}Na_{0.44}Ba_{0.04}Ni_{0.02}Nb_{0.98}O_{2.98}$) annealed at different temperatures for different durations, and in various atmospheres. Structural, microstructural, and chemical analyses suggest that vacuum, N_2, and O_2 atmospheres promote the growth of the TB phase from the sample surface, of which the thickness increases with annealing temperature and duration. In contrast, annealing in air does not promote such growth due to lower evaporation of K and Na. Among all atmospheres, the growth starts the earliest, i.e., at 800 °C, in vacuum compared to that as late as 1000 °C in O_2. The association of growth of the TB phase with the degree of alkali volatilization that is dependent on the atmosphere, and that with the resultant variation in diffusion rate, uncovers the formation mechanism of the beneficial interface that may also be applicable to other KNN-based materials for advanced photoferroelectric applications.

1. Introduction

The (K,Na)NbO_3 (KNN) perovskite structure is a solid solution of ferroelectric $KNbO_3$ and antiferroelectric $NaNbO_3$. KNN presents an orthorhombic phase at room temperature and experiences orthorhombic-tetragonal and then tetragonal-cubic phase transitions as the temperature increases.[1] Among others, KNN can be modified by $BaZrO_3$,[2] (Bi, Na, K)ZrO_3,[3] and (Bi, Na)TiO_3,[4] and thus constructs morphotropic phase boundaries (MPB) between tetragonal and rhombohedral phases around room temperature. A common issue for sintered KNN is stoichiometric deviation caused by the hygroscopic and volatile nature of K and Na, which ends up with the formation of secondary phases, such as the tungsten bronze phase that are considered detrimental to the piezoelectric properties.[5] KNN-based piezoceramics are lead-free and have attracted research interest owing to their good ferroelectric and piezoelectric performance comparable to those of the lead-based counterparts. For instance, excellent piezoelectric coefficient (d_{33}) values of 416 pC/N and 704 pC/N, which are comparable to that of the Pb(Zr,Ti)O_3 (PZT) based compositions, have been achieved in textured (K,Na,Li)(Nb,Ta,Sb)O_3[6] and (K,Na)(Nb,Sb)O_3—$CaZrO_3$—(Bi,K)HfO_3 ceramics,[7] respectively. Compared to other lead-free piezoceramics, KNN-based ceramics usually exhibit better temperature stability in terms of piezoelectric properties,[8] a larger mechanical quality factor (Q_m),[9] and better fatigue resistance.[10,11] These advantages make

X. Shi, M. Kuhfuß, N. H Khansur
Institute of Glass and Ceramic
Department of Materials Science and Engineering
Friedrich-Alexander-Universität Erlangen-Nürnberg (FAU)
91058 Erlangen, Germany
E-mail: xi.shi@fau.de; neamul.khansur@fau.de

The ORCID identification number(s) for the author(s) of this article can be found under https://doi.org/10.1002/aelm.202300601

DOI: 10.1002/aelm.202300601

Y. Bai
Microelectronics Research Unit
Faculty of Information Technology and Electrical Engineering
University of Oulu
Oulu 90570, Finland

C. Wichmann, M. Moritz, C. Papp
Lehrstuhl für Physikalische Chemie II
Friedrich-Alexander-Universität Erlangen-Nürnberg (FAU)
91058 Erlangen, Germany

C. Papp
Angewandte Physikalische Chemie
Freie Universität Berlin
14195 Berlin, Germany

KNN-based piezoceramics potential candidates as substitutes for lead-based piezoelectric components such as sensors, actuators, and transducers for applications in electronics, motor vehicles, and medical diagnosis.[12-15]

Similar to other polar perovskite oxides, most KNN-based ceramics have a wide bandgap of >3 eV. Photoferroelectric materials, on the other hand, are those materials that exhibit both photovoltaic and ferroelectric effects[16] for which a lower bandgap is crucial for visible range absorption to ensure good photovoltaic performance. Reducing the bandgap whilst retaining good ferroelectric and piezoelectric properties could make KNN-based ceramics also an interesting candidate for photoferroelectric applications[16,17] such as phototransistor,[18] photoswitch,[19] photo field-effect transistor,[20] light-effect transistor,[21] monolithic solaristor,[18] *etc*. An effective method to reduce the bandgap of KNN is doping the B-site with non-d^0 transition metal cations and, in the meantime, creating oxygen vacancies ($V_O^{\cdot\cdot}$). For instance, doping $(K_{0.5}Na_{0.5})NbO_3$ with as low as 2 mol% $Ba(Ni_{1/2}Nb_{1/2})O_{3-\delta}$ (BNNO) can result in a reduced bandgap of <2 eV from over 3.8 eV, due to the eased charge transfer from, or to, Ni 3*d* states in the newly introduced Ni^{2+}- $V_O^{\cdot\cdot}$ defect dipoles.[22–24] The drawback of such a doping method is that the concentrations of both Ni^{2+} and $V_O^{\cdot\cdot}$ must be precisely controlled so that the bandgap reduction does not significantly alter distortion of the crystal structure.[17] Ferroelectric and piezoelectric properties vanish upon a significant alteration of structural distortion. However, as mentioned above, KNN has the common issue of off-stoichiometry, which makes precise control of the dopant concentration difficult.[25]

Nevertheless, it has been found that by introducing >5 mol % A-site deficiency in the starting reactants of the $(K_{0.5}Na_{0.5})NbO_3$-BNNO composition, a polar tetragonal tungsten bronze $(K,Na,Ba)_\alpha(Ni,Nb)_\beta O_\gamma$ phase (TTB) (<20 mol%) forms alongside the orthorhombic perovskite $(K, Na, Ba)_x(Ni, Nb)_yO_z$ phase (>80 mol %). Contrary to the detrimental secondary phases formed in other KNN-based ceramics, the TTB phase here is proven beneficial, as a special interface that is referred to as a pseudo-morphotropic phase boundary (pseudo-MPB) is formed between the perovskite and TTB phases. This pseudo-MPB helps to reduce the bandgap by 1–2 eV as well as to optimize the ferroelectric and piezoelectric properties.[22] Designing A-site deficiency has become a favored method as it not only relaxes the strict requirement for the stoichiometry of the starting reactants but also offers to create and tune the pseudo-MPB during post-sintering thermal treatment.[17] The previous study has found that the TTB phase can further grow from small tungsten bronze "seeds" already existing in highly A-site deficient (10–15 mol %) samples or can emerge from "seed-free", pure perovskite samples with lower A-site deficiency (<5 mol %) via annealing in N_2 and O_2 atmosphere. Loss of K and/or Na during annealing is thought to be the reason for the growth or emergence of the TTB phase.[17]

However, the growth mechanism of the TTB phase from the perovskite phase is still unclear at this stage. Further understanding requires to study possible influential factors that promote the TTB phase to appear from the "seed-free" samples. In this work, the growth of the TTB phase in an A-site deficient KNBNNO ceramic under different annealing conditions, including various atmospheres and annealing temperatures and periods, is systematically analyzed. Characterization methods, including SEM (scanning electron microscopy), XPS (X-ray photoelectron spectroscopy), and XRD (X-ray diffraction) are deployed, from which the growth mechanism of the TTB phase is clarified. This study guides bandgap engineering of KNN-based ceramics via the construction of the pseudo-MPB for photoferroelectric applications benefiting from building advanced interfacial configurations in a controlled manner.

2. Results and Discussions

Figure 1 shows the XRD patterns collected from the surface of the unannealed KNBNNO sample and those annealed in O_2, air, N_2, and vacuum at 1000 °C for 8 h. Reflections assigned to the TTB phase are marked in the figure. The unannealed sample contained a single perovskite phase, which was confirmed using Le bail fitting. This perovskite phase was best modeled as an *Amm*2 (orthorhombic) space group with lattice parameters of a ≈3.965 Å, b ≈5.635 Å, and c ≈5.664 Å. This is consistent with the result in the previous work. Differently, reflections assigned to a TTB phase, in addition to the perovskite phase mentioned above, were observed for samples annealed in vacuum, N_2, and O_2 (Figure 1b). This TTB phase was also confirmed by Le bail fitting, being modeled as a *P4bm* (polar tetragonal) space group.[17,22] It is to be noted that the presence of the TTB phase altered unit cell parameters of the perovskite phase, with the evidence of unit cell volume and crystal structure distortion tending to decrease as the TTB phase grew. This speculates the influence of the TTB phase growth on the spontaneous polarization of perovskite unit cells. Nevertheless, observations in previous works suggest that during sintering, the perovskite phase might have formed before the TTB phase with the mass transfer of Na and K. The rest of the reactants would form the TTB phase as it failed to satisfy the stoichiometry required for the perovskite phase.[17,22]

By comparing the intensities of the reflections belonging to the TTB phase, it could be estimated that a larger amount of the TTB phase was possibly formed in the N_2-annealed sample than that in the O_2-annealed sample. This observation contradicts the previous study in which a larger amount of the TTB phase was formed in O_2-annealed samples than in N_2-annealed samples due to possibly faster migration of K and Na in forms of K_2O and Na_2O in the O_2 atmosphere,[17] as will be discussed below. For the sample annealed in air, no noticeable evidence for the possible existence of the TTB phase was found. Such an observation was also supported by the fact that the unannealed sample and sample annealed in the air generally exhibited a translucent green color, while the samples annealed in vacuum, O_2, and N_2 changed to a more opaque, darker color (See Figure S1, Supporting Information). The different extents of transparency reflected the difference in the amount of TTB phase present in the samples. The difference between the annealed samples implies that the diffusion rates of Na and K from the perovskite phase, thus triggering the formation of the TTB phase, were likely faster in vacuum and N_2 atmosphere, but they were slower in air atmosphere.

To study the distribution of the TTB phase grown in different atmospheres, **Figure 2** shows cross-sectional SEM images taken from the samples annealed in air, O_2, N_2, and vacuum at 1000 °C for 2 and 8 h. The perovskite phase was seen darker in the SEM

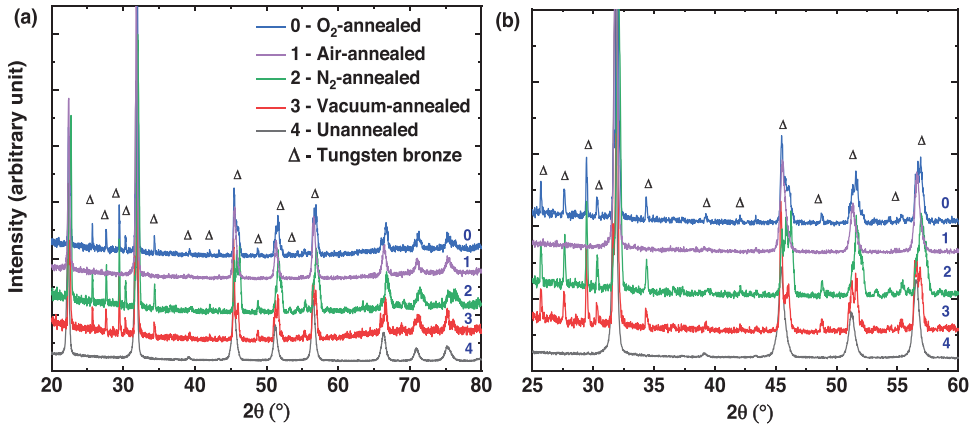

Figure 1. Surface XRD patterns of the unannealed KNBNNO ceramic sample and the ones annealed in O_2, air, N_2, and vacuum at 1000 °C for 8 h: a) for full range and b) for enlarged 2θ range of 25°–60°. Reflections assigned to the TTB phase are marked.

image, contrasting with the brighter TTB phase. Grains of the TTB phase appeared as densely distributed bright spots close to the surface and were sporadically allocated along the depth of the sample.

After careful examination, no TTB phase was found in any sample annealed in air for 2 and 8 h (Figure 2a,e). The sample annealed in air stayed identical to the unannealed sample in which a single perovskite phase was also confirmed in previous studies.[17,22] This observation came as a surprise because 800 °C is considered to be the theoretical temperature that can trigger the diffusion and hence loss of K and Na, which should create a favorable environment for the formation of the TTB phase.[17] For samples annealed in O_2, the TTB phase was found only after being annealed at 1000 °C (Figure 2b,f). However, no new phase was formed in samples annealed at 800 and 900°C in O_2. The N_2 atmosphere played a similar role to that of the O_2 atmosphere for the emergence and growth of the TTB layer when annealing the samples for 2 and 8 h at 1000 °C (Figure 2c,g). For samples annealed in vacuum, the TTB layer started to form already at 800 °C after being annealed for 2 h, and the layer could be seen in all samples annealed at 800–1000 °C for 2 and 8 h (see Figure 2d,h; Figure S2, Supporting Information).

Except for air-annealed samples with no TTB layer (it could be argued that the white dots in Figure 2e are TTB phases, while the concentration is quite minor and the thickness could not be measured), the TTB concentration as a function of the distance to the surface is plotted in Figure 2 i–n. The TTB thickness is evaluated based on the sample area with a TTB concentration of ≥ 10% (see the blue dotted lines in Figure 2i–n) and is discussed in detail in **Figure 3**. Regardless of annealing times, the TTB concentration at the surface for vacuum and O_2-annealed samples was all ≈20% and generally declined with depth. It is noted that the increasing trend at ≈85–90 µm inward the sample surface in Figure 2k could be due to errors from image analysis caused by similar contrasts of the TTB and the perovskite phase. The 2 h-annealed samples showed an abrupt decline in TTB concentration away from the surface, while for 8 h-annealed samples the TTB layers grew deeper. For N_2-annealed samples, the TTB concentration at the surface was also significantly higher than other samples annealed in other conditions (i.e., 40% for the 8 h-annealed sample, see Figure 2m). Nevertheless, the significantly high TTB concentration close to the interface (≈80%) for the 2 h-annealed sample (see Figure 2j), as well as the concentration fluctuation in the 8-hour-annealed sample (see Figure 2m), could be due to the pores and surface impurities with the same contrast as TTB, which affected accurate concentration calculation. Overall, it is suspected that the TTB layer grows from the surface, reaching a concentration of 20% to 40% (depending on the atmosphere) and then gradually spreading deeper inward with elongated annealing time.

This evidence indicates that the post-sintering annealing atmosphere played a decisive role in the formation of the TTB layer, and temperature influenced the growing process. This can be witnessed in the comparison between samples annealed in vacuum where the TTB phase already started to grow at 800 °C (See Figure S2, Supporting Information) and those, annealed in O_2, where the TTB phase was formed only at a sufficiently high temperature of 1000 °C. Regarding the air atmosphere, possible growth of the TTB phase could not be excluded if the annealing temperature or period was further increased. However, further increasing the annealing temperature would approach the samples' sintering temperature (1150 °C), making the post-sintering annealing procedure less meaningful in practice as a perovskite-TTB composite could have been fabricated solely during sintering.[17,22]

To provide a quantitative overview of the TTB phase, the growth of the TTB layer (area with TTB concentration ≥ 10%) in annealed samples at different conditions is presented in Figure 3a,b. For samples annealed in vacuum (see Figure 3a), the layers varied from an insignificant growth of 1.5 µm thick at 800 °C for 2 h to ≈39.8 µm thick at 1000 °C for 8 h. Overall, higher annealing temperature and/or longer annealing period tended to result in a thicker TTB layer due to the increasing vapor pressure values of K and Na with the temperature increase.[26] Similar trends were seen for samples annealed in other atmospheres, see Figure 3b for the evolution of TTB layers of samples annealed in O_2, N_2, and vacuum at 1000 °C for different annealing times. The layers in samples annealed in N_2 were thickest, i.e., 16.2, 25.9, and 78.9 µm for annealing periods of 2, 4, and 8 h, respectively. For O_2-annealed samples, the layers were ≈9.9, 29.7, and 39.6 µm for annealing periods of 2, 4, and 8 h, respectively. With

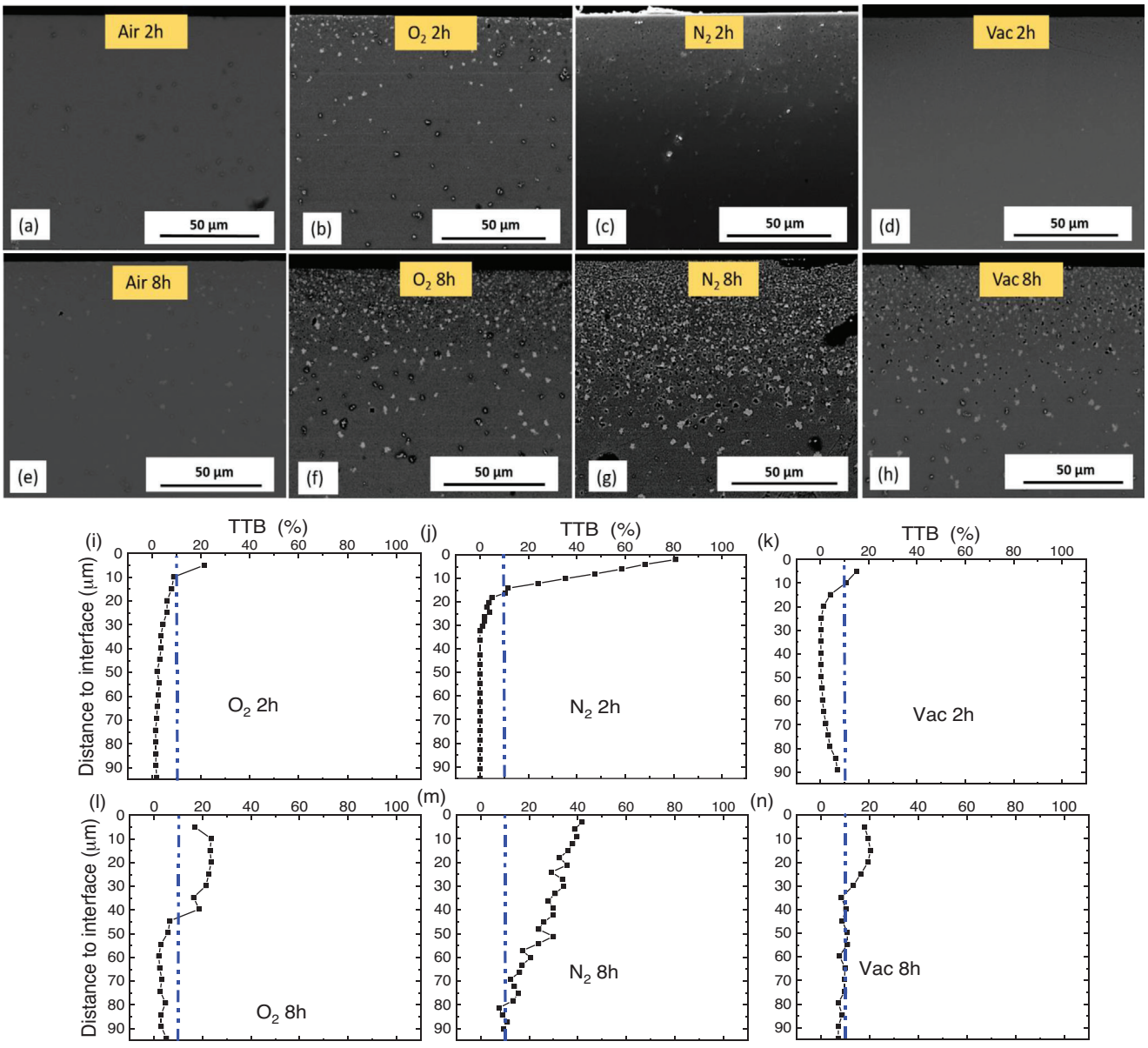

Figure 2. Cross-sectional SEM micrographs of KNBNNO ceramic samples annealed in a,e) Air, b,f) O_2, c,g) N_2, and d,b) vacuum at 1000 °C for a–d) 2 h and e–h) 8 h. For O_2, N_2 and vacuum annealed samples, Figure 2 i–n showed the TTB concentration with the dependence of distance from sample interface. The blue dotted lines defined that the regions of a valid TTB layer, where the TTB concentration is ≥ 10%.

consideration of calculation errors, it is found that at 1000 °C the TTB layers tend to grow at a similar rate in vacuum and O_2 conditions. In contrast, N_2 seemed to provide a more favorable environment for its growth, where the TTB layer grown at 1000 °C for 8 h was almost as twice thick as those annealed in vacuum and O_2. Nevertheless, the nonexistence of TTB layers in samples at lower annealing temperatures or fewer hours in O_2 confirmed the above-mentioned hypothesis of easier formation and growth of TTB layer in vacuum and N_2 than in O_2. The origin of a thicker TTB layer for N_2-annealed sample may be affected by reduced concentrations of K at the surface. This is supported by the XPS data and previous works which indicate that the formation of the TTB phase could have been accelerated by the variation in K/Na ratio from their stoichiometric ratio, i.e., K on the sample surface was replaced by the Na during the N_2 annealing.

To understand the dynamics of the alkali elements, the annealed samples were further investigated using XPS. Spectra were collected from samples annealed at 1000 °C for 2 h in air, O_2, and N_2 atmosphere. Results for the K 2*p* region are shown in **Figure 4**. The air-annealed sample showed two major peaks at 295.7 and 292.9 eV. The peak at 292.9 eV also contained shoulders at higher and lower binding energy. These results are in agreement with previous XPS data of KNN ceramics.[27] The two major peaks, fit in the green curves (Figure 4a), are attributed to the spin-orbit-splitting of the K 2*p* orbitals of non-crystalline K_2O.[28] The two shoulders, which are fitted by the blue curves (Figure 4a)

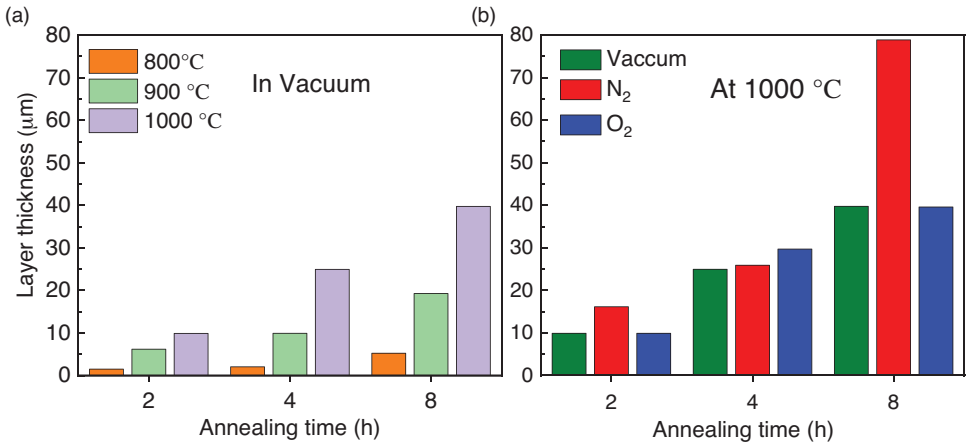

Figure 3. Layer thickness of tungsten bronze phase for a) samples annealed in vacuum for 2, 4, and 8 h at 800, 900, and 1000 °C and b) samples annealed at 1000 °C for 2, 4, and 8 h in vacuum, N_2, and O_2.

at 291.4 and 294.2 eV represent signals from K in the perovskite structure. Due to the high surface sensitivity of XPS, the intensity ratio of the two species might imply their locations in the sample. Therefore, the less pronounced contributions of K from the perovskite lattice in the XP spectra suggests a higher abundancy in the bulk of the sample. According to the quantification, 34% of the sampled volume (<10 nm) was assigned to K, where 22% and 12% were attributed to K_2O and K in the perovskite, respectively. A similar spectrum was obtained from the sample annealed in O_2 atmosphere (Figure 4b). The overall concentration of K slightly decreased to 29%, consisting of 19% attributed to K_2O and 10% attributed to K in the perovskite. This indicated a thinner K_2O layer at the sample surface. After being annealed in N_2 atmosphere, the intensity of the K signals drastically decreased (Figure 4c). The overall concentration of K was reduced to 4.7%. Meanwhile, signals corresponding to Na started to grow to a similar surface concentration as K in air and O_2 annealed samples, (i.e., 36%, see Figure S3 and Table S1, Supporting Information). Apparently, K on the sample surface was replaced by Na during annealing in N_2. Also, the signals in blue (Figure 4c), corresponding to the perovskite, further increased with respect to the K_2O. After annealing in N_2 atmosphere, 1.6 % out of the 4.7% K was attributed to the perovskite. The data thus suggest that the removal of K and the agglomeration of Na at the surface is beneficial for the formation of the TTB phase. Overall, it should be mentioned that the current work highlights the different degrees of alkali volatilization and associated growth in surface TTB phase; however, oxygen vacancy and associated defect mechanisms should also be considered for a better understanding the photoferroelectric properties of these materials.

3. Conclusion

To pave the way toward controlled construction of the perovskite-tungsten bronze phase interface for advanced opto-ferroelectric and opto-piezoelectric applications, $K_{0.50}Na_{0.44}Ba_{0.04}Ni_{0.02}Nb_{0.98}O_{2.98}$ (KNBNNO) ceramic has been studied in this work in terms of understanding formation and growth of the tungsten bronze phase from pure perovskite phase via a post-sintering annealing process. Ceramic samples have been fabricated and then annealed in vacuum, N_2, O_2, and air atmosphere at 800–1000 °C for 2–8 h. A newly grown tungsten bronze phase with different thicknesses has been found at the surface of the pure perovskite phase after being annealed in

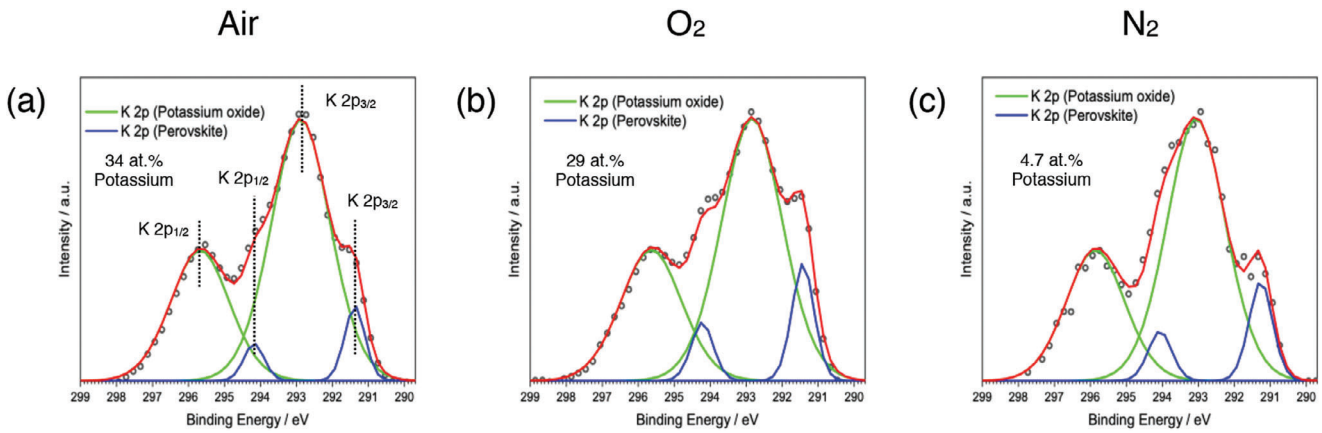

Figure 4. XPS results with an excitation energy of 1486.6 eV for the KNBNNO samples annealed in a) air, b) O_2, and c) N_2 at 1000 °C for 2 h.

N_2, O_2, and vacuum, whereas the new phase has not formed during annealing in air. Evidence has shown that the formation temperature of the tungsten bronze phase could be as low as 800 °C in vacuum whilst as high as 1000 °C in O_2 with a positive relationship between annealing temperature/period and thickness of the newly formed tungsten bronze phase. Analyses of this study indicate that the growth of the tungsten bronze phase is determined by the different degrees of volatilization rate of K and Na in certain atmospheres. More volatile K_2O appears in vacuum and N_2 upon the KNBNNO perovskite phase being heated, while this process is slower in O_2 and negligible in air given the same annealing temperature and period. This finding provides guidance to future works on bandgap engineering through microstructural design and manipulation for perovskite photoferroelectric materials based on alkali niobates.

4. Experimental Section

$K_{0.50}Na_{0.44}Ba_{0.04}Ni_{0.02}Nb_{0.98}O_{2.98}$ (KNBNNO) ceramic samples that were designed to have 2 mol% A-site deficiency were fabricated with a conventional solid-state reaction method. K_2CO_3 (≥ 99%, J.T. Baker, USA), Na_2CO_3 (≥ 99%, Sigma–Aldrich, USA), $BaCO_3$ (99.98%, Aldrich Chemistry, USA), NiO (99.999%, Aldrich Chemistry, USA), and Nb_2O_5 (99.9%, Aldrich Chemistry, USA) powders were weighed according to the stoichiometry, which was counterchecked by an X-ray fluorescence spectrometer (XRF, Axios max 4 kW, PANalytical, UK). After ball milling, the dried powder was calcined at 825 °C for 4 h in air. The calcined powder was milled for the second time before being uniaxially pressed into green bodies and eventually sintered at 1150 °C for 2 h in air. Previous works can be referred to for fabrication details.[17,22]

Sintered ceramic samples were polished to 500–600 μm thick, and then each sample was cut into several 4 mm × 4 mm square-shaped pieces using a diamond wire saw (DWS175 Diamond WireTec GmbH & Co.KG, Germany). The cut samples were annealed under different conditions: i) vacuum, air, N_2, or O_2 atmosphere, ii) at 800, 900, or 1000 °C, and iii) for 2, 4, or 8 h. An atmospheric oven connected to corresponding gas cylinders was used to carry out the annealing and the heating and cooling rates were kept at 5 K min^{-1}.

A total number of 30 annealed samples were studied. SEM (Quanta 200, FEI Co., USA) was used to characterize the cross-sectional surface of annealed samples. Software ImageJ was used to evaluate the thickness of different compound layers observed in the samples. The cross-section SEM image at the depth direction was divided by rectangular slices with the same width (2–5 μm) and the TTB concentration of each small region was estimated. The area with TTB concentration of ≥ 10% is regarded as the TTB layer, which is the criteria for measuring the TTB layer thickness. The XRD patterns were collected from the sample surface using a D8 Advance diffractometer (Bruker AXS GmbH, Germany). XPS (ESCALAB 250Xi, Thermo Fisher Scientific, USA) was also carried out on the sample surface with an Al Kα source (spot size of 500 μm) and a CEM (channel electron multiplier) detector. Prior to XPS measurement, the sample surfaces were cleaned by an Ar cluster gun. The XP spectra were fitted with CasaXPS (V 2.3.18PR1.08) using Voigt functions (GL(30)). Linear backgrounds were subtracted in all spectra. The obtained integrated peak area (A_i) was corrected using an inelastic mean free path (IMFP, λ_i), photoionization cross-section (σ_i), and kinetic energy (E_{kin}) of the emitted photoelectron:

$$A_i' = \frac{A_i \times E_{kin}}{\lambda_i \times \sigma_i} \quad (1)$$

where A_i' is the corrected area. λ_i and σ_i values were obtained from the TPP-2 M algorithm with SESSA (Version 1)[29] and from the atomic and nuclear data tables.[30,31]

Supporting Information

Supporting Information is available from the Wiley Online Library or from the author.

Acknowledgements

X.S. acknowledges the support from ETI-funding of Friedrich-Alexander-Universität Erlangen-Nürnberg. Neamul H. Khansur gratefully acknowledges the financial support for this work from the Deutsche Forschungsgemeinschaft under KH 471/2 . M.K., X.S., and N.H.K. acknowledge financial support from the Deutsche Forschungsgemeinschaft under GRK2495/F/H. This work was financially supported by the Research Council of Finland (grant number 24302332). The authors acknowledge the Centre for Material Analysis of the University of Oulu for the use of their facilities and electrode fabrication. N.H.K. acknowledges financial supprot by Deutshce Froschungsgemeinschaft and Friedrich-Alexander-Universität within the funding program "Open Access Publication Funding". Research Council of Finland, Grant/Award Number: 24302332; Deutsche Forschungsgemeinschaft, Grant/Award Number:KH 471/2 and GRK2495; Friedrich-Alexander-Universität Erlangen-Nürnberg.

Conflict of Interest

The authors declare no conflict of interest.

Data Availability Statement

The data that support the findings of this study are available in the supplementary material of this article.

Keywords

(K, Na)NbO3 perovskite, photoferroelectric applications, tetragonal tungsten bronze phase

Received: September 5, 2023
Revised: November 3, 2023
Published online: December 7, 2023

[1] J. Rödel, W. Jo, K. T. P. Seifert, E.-M. Anton, T. Granzow, D. Damjanovic, *J. Am. Ceram. Soc.* **2009**, *92*, 1153.
[2] R. Wang, K. Wang, F. Yao, J.-F. Li, F. H. Schader, K. G. Webber, W. Jo, J. Rödel, *J. Am. Ceram. Soc.* **2015**, *98*, 2177.
[3] X. Wang, J. Wu, D. Xiao, J. Zhu, X. Cheng, T. Zheng, B. Zhang, X. Lou, X. Wang, *J. Am. Ceram. Soc.* **2014**, *136*, 2905.
[4] T. Karaki, T. Katayama, K. Yoshida, S. Maruyama, M. Adachi, *Jpn. J. Appl. Phys.* **2013**, *52*, 09KD11.
[5] B. Malic, J. Koruza, J. Hrescak, J. Bernard, K. Wang, J. Fisher, A. Bencan, *Mater* **2015**, *8*, 8117.
[6] Y. Saito, H. Takao, T. Tani, T. Nonoyama, K. Takatori, T. Homma, T. Nagaya, M. Nakamura, *Nature* **2004**, *432*, 84.
[7] P. Li, J. Zhai, B. Shen, S. Zhang, X. Li, F. Zhu, X. Zhang, *Adv. Mater.* **2018**, *30*, 1705171.
[8] K. Shinekumar, S. Dutta, *J. Electron. Mater.* **2015**, *44*, 613.
[9] B. C. Park, I. K. Hong, H. D. Jang, V. D. N. Tran, W. P. Tai, J.-S. Lee, *J. Mater. Sci. Lett.* **2010**, *64*, 1577.
[10] F.-Z. Yao, E. A. Patterson, K. Wang, W. Jo, J. Rödel, J.-F. Li, *Appl. Phys. Lett.* **2014**, *104*, 242912.

[11] F.-Z. Yao, K. Wang, Y. Shen, J.-F. Li, *J. Appl. Phys.* **2015**, *118*, 134102.
[12] A. M. Vommi, T. K. Battula, *Expert Syst. Appl.* **2023**, *218*, 119612.
[13] B. Wang, G. Huangfu, Z. Zheng, Y. Guo, *Adv. Funct. Mater* **2023**, *33*, 2214643.
[14] S.-W. Zhang, Z. Zhou, J. Luo, J.-F. Li, *Ann. Phys.* **2019**, *531*, 1800525.
[15] J. Ou-Yang, B. Zhu, Y. Zhang, S. Chen, X. Yang, W. Wei, *Appl. Phys. A* **2015**, *118*, 1177.
[16] D. Wang, G. Wang, Z. Lu, Z. Al-Jlaihawi, A. Feteira, *Front. Mater. Sci.* **2020**, *7*, 91.
[17] Y. Bai, C. Prucker, N. H. Khansur, *J. Am. Ceram. Soc.* **2022**, *105*, 3364.
[18] A. Pérez-Tomás, A. Lima, Q. Billon, I. Shirley, G. Catalan, M. Lira-Cantú, *Adv. Funct. Mater.* **2018**, *28*, 1707099.
[19] F. P. García de Arquer, A. Armin, P. Meredith, E. H. J. N. R. M. Sargent, *Nat. Rev. Mater.* **2017**, *2*, 1.
[20] D. Kufer, G. Konstantatos, *ACS Photonics* **2016**, *3*, 2197.
[21] J. K. Marmon, S. C. Rai, K. Wang, W. Zhou, Y. Zhang, *Front. Phys.* **2016**, *4*, 8.
[22] Y. Bai, A. A. Kistanov, W. Cao, J. Juuti, *J. Phys. Chem. C* **2021**, *125*, 8890.
[23] Y. Bai, P. Tofel, J. Palosaari, H. Jantunen, J. Juuti, *J. Adv. Mater.* **2017**, *29*, 1700767.
[24] I. Grinberg, D. V West, M. Torres, G. Gou, D. M. Stein, L. Wu, G. Chen, E. M. Gallo, A. R. Akbashev, P. K. Davies, J. E. Spanier, A. M. Rappe, *Nature* **2013**, *503*, 509.
[25] T. Rojac, M. Kosec, B. Malič, J. Holc, *Sci. Sinter.* **2005**, *37*, 61.
[26] A. Popovic, L. Bencze, J. Koruza, B. Malic, *RSC Adv.* **2015**, *5*, 76249.
[27] L. Wang, W. Ren, P. Shi, X. Wu, *J. Alloys Compd.* **2014**, *608*, 202.
[28] L. Wang, K. Yao, P. C. Goh, W. Ren, *J. Mater.* **2009**, *24*, 3516.
[29] S. Tanuma, C. J. Powell, D. R. Penn, *Surf. Interface Anal.* **2003**, *35*, 268.
[30] M. B. Trzhaskovskaya, V. I. Nefedov, V. G. Yarzhemsky, *Data Tables* **2001**, *77*, 97.
[31] M. B. Trzhaskovskaya, V. I. Nefedov, V. G. Yarzhemsky, *Data Tables* **2002**, *82*, 257.